Size-Controlled Synthesis of LiFePO₄/C Composites as Cathode Materials for Lithium Ion Batteries

Jiali Liu[1], Zhangzhi Wang[2], Guohua Zhang[2], Yun Liu[2], Aishui Yu[1,]*

[1] Department of Chemistry and Shanghai Key Laboratory of Molecular Catalysis and Innovative Materials, Institute of New Energy, Fudan University, 2205 Songhu Road, Shanghai 200433, China
[2] Hangzhou Golden Horse Energy Technology Co., LTD, Xiaoshan Economic and Technology development zone, 117 Hongxing Road, Hangzhou 311200, China
[*]E-mail: asyu@fudan.edu.cn

Nano-micro-structured spherical LiFePO₄/C composite is synthesized via a ball-milling-assisted spray-drying method. SEM characterization demonstrates that the primary and secondary particle sizes are on the order of several hundred nanometers and approximately fifteen microns. The primary particles are successfully controlled through homogenous milling with a narrow particle size distribution. Herein, LiFePO₄/C composites with a primary particle (i.e., 200 nm and 400 nm in diameter) are prepared. The relationship between electrochemical performance and particle size is evaluated using both half- and full-cell tests. The results demonstrate that the 200 nm diameter sample has a better rate capability and low-temperature performance, whereas the 400 nm sample is better at cycling.

1. INTRODUCTION

Currently, high-power batteries for electric vehicles and hybrid electric vehicles are in demand because they are advantageous for the environment and renewable energy [1, 2]. Lithium ion batteries with olivine-structured LiFePO₄ as the cathode material are the most promising candidates for an energy storage system in these applications [3-5]. However, the intrinsic disadvantages of poor electronic conductivity and a low ionic diffusion constant prevent its application [6-8]. To overcome these barriers, many studies have been proposed to improve electrochemical behavior of LiFePO₄, such as nano-size preparation, carbon coating, and doping with supervalent cations [9-12]. Based on such studies, many synthesis routes, such as solid-state reactions, the sol-gel method, and hydrothermal

processes, have been employed to prepare a nano-size $LiFePO_4$/composite to improve electrochemical performance [13-15].

Currently, the solid-state method is the most promising route for $LiFePO_4$ production [16]; however, it is difficult to control morphology and particle size distribution using this method. It is well-known that ball-milling can reduce particle size and that spray-drying can generate micro-spheres with a narrow size distribution [17, 18]. Lu et al. explored the ball-milling-assisted spray-drying method to synthesize micron-size spherical $LiFePO_4$/C composites. However, certain particles with irregular morphologies were observed [19]. They then observed that by adding PEG-400 in the starting material, the primary particle was more uniform [5]. Z. X. Liang analyzed the effect of a carbon source on the microstructure of an $LiFePO_4$/C composite generated through spray-drying; the organic carbon source had a more uniform morphology compared with inorganic sources [20].

Herein, we also prepared the precursor through a ball-milling-assisted spray-drying method. The SEM photos suggested that a nano-microstructured spherical morphology with a narrow size distribution remained even after heat treatment. The primary particle size that determines electrochemical performance, including cycling, rate capability, and low-temperature performance, could be successfully controlled via this method. Hence, this would be the most promising method for commercial production of $LiFePO_4$/C directed to hybrid electrical vehicles and pure electrical vehicle markets.

2. EXPERIMENTAL

2.1 Material synthesis

The $LiFePO_4$/C composite was prepared using a wet ball-milling procedure, followed by spray-drying and solid-state calcination. Stoichiometric levels of LiH_2PO_4 (Sichuan Tianqi Lithium Industries, Inc.) and Fe_2O_3 (Sinopharm Chemical Reagent Co. Ltd., Shanghai, AR) with a certain quantity of sucrose (Sinopharm Chemical Reagent Co. Ltd., Shanghai, AR) were dispersed in alcohol and wet ball-milled for 15 h. The resulting stable suspension was then dried to form a mixed precursor via a spray drier with hot air at 0.1 MPa. This prepared powder was transferred to a tube furnace and heated to 350 °C for 5 h under nitrogen (99.9%) and then elevated to 700 °C for 10 h under the same atmosphere.

2.2 Physical characterization

X-ray diffraction (XRD) was performed using a Bruker D8 Advance X-ray diffraction spectrometer with a Cu Kα radiation source (λ=1.5406 Å) and a 4 ° min^{-1} step size from 10 to 80 °. The powder morphology was observed using a scanning electron microscope (SEM) (JEOL JSM-6390). The carbon content in the $LiFePO_4$/C composite was measured using a carbon-sulfur analyzer (Eltra CS800). The specific surface area of the powder particles was measured using the Brunauer–Emmett–

Teller (BET) method (GeminiV-2380). The particle size distribution was analyzed using a Zetasizer. The interior structure of the carbon-coated LFePO$_4$ particles was observed through transmission electron microscopy (TEM, JEOL. Ltd., JEM-2010F).

2.3 Electrochemical measurements

2.3.1 Half-cell tests

Electrodes were constructed using a mixture of LiFePO$_4$/C composite (85 wt%), carbon black (7.5 wt%) and polyvinylidene fluoride in N-methylpyrrolidinon (7.5 wt%). The slurry was spread onto Al foil and dried at 80 °C under a vacuum; then, it was roll-pressed prior to use. The electrochemical properties were measured using a CR 2016 coin-type cell with lithium as the anode material. The electrolyte used was 1 M LiPF$_6$ in ethylene carbonate (EC), diethylene carbonate (DEC) and methyl ethylene carbonate (EMC) (EC/DEC/ EMC= 1:1:1 V/V/V). A Celgard 2325 PP/PE/PP membrane was used as a separator. The charge-discharge measurements were performed using an automatic galvanostatic unit (Neware, Shenzhen, China) at 0.2 C from 2.0-4.0 V.

2.3.2 Full cell tests

To investigate rate capability, long-term cycling and low-temperature performance for the electrode, an IFR26650E-3000-type full cell was assembled. The anode electrode was commercial graphite (CMB 340, BTR CO. LTD) and polyvinylidene fluoride in N-methylpyrrolidinon (7.5 wt%) at an 87:13 ratio (weight). The slurry was spread onto copper foil. The electrolyte and separator types were the same as for the half cells. Electrochemical performance was measured at various rates and at 2.0-3.6 V.

3. RESULTS AND DISCUSSION

3.1 Physical characterization

A series of parameters were adjusted during the production process to control the sample particle size. The typical 200 nm- and 400 nm-diameter primary particles that are illustrated as examples herein are labeled as LFP-400 and LFP-200. Fig. 1 a) and b) show the XRD patterns for LFP-400 and LFP-200, respectively. The sharp diffraction peaks, which were consistent with the standard olivine-structured LiFePO$_4$ (PDF card NO. 40-1499), indicate a high level of sample crystallization and no impurities.

The morphologies of the LiFePO$_4$/C composites were investigated using SEM. Fig. 2 a) shows the panoramic morphologies for LFP-400; this synthesis method can produce LiFePO$_4$/C microspheres with a fairly uniform size distribution (5-10 μm). A detailed investigation of the microsphere is shown in Fig. 2 b); the microspheres were composed of primary particles approximately 400 nm in diameter,

and homogeneous pores were observed on the microsphere surface. Fig. 2 c) shows the spherical morphology for the LFP-200 sample, and an enlarged image is shown in Fig. 2 d). Similar to LFP-400, the regular spherical particles comprised 200 nm-diameter LiFePO$_4$/C particles, and homogenous pores were formed in this sample.
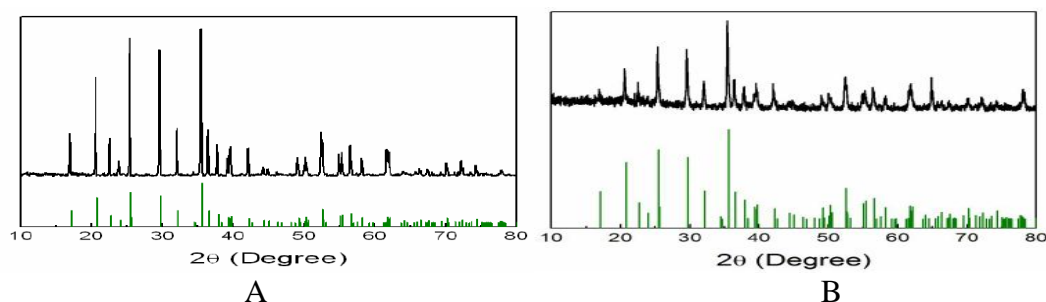

Figure 1. XRD patterns for the LiFePO$_4$/C composite; a) LFP-400, b) LFP-200.
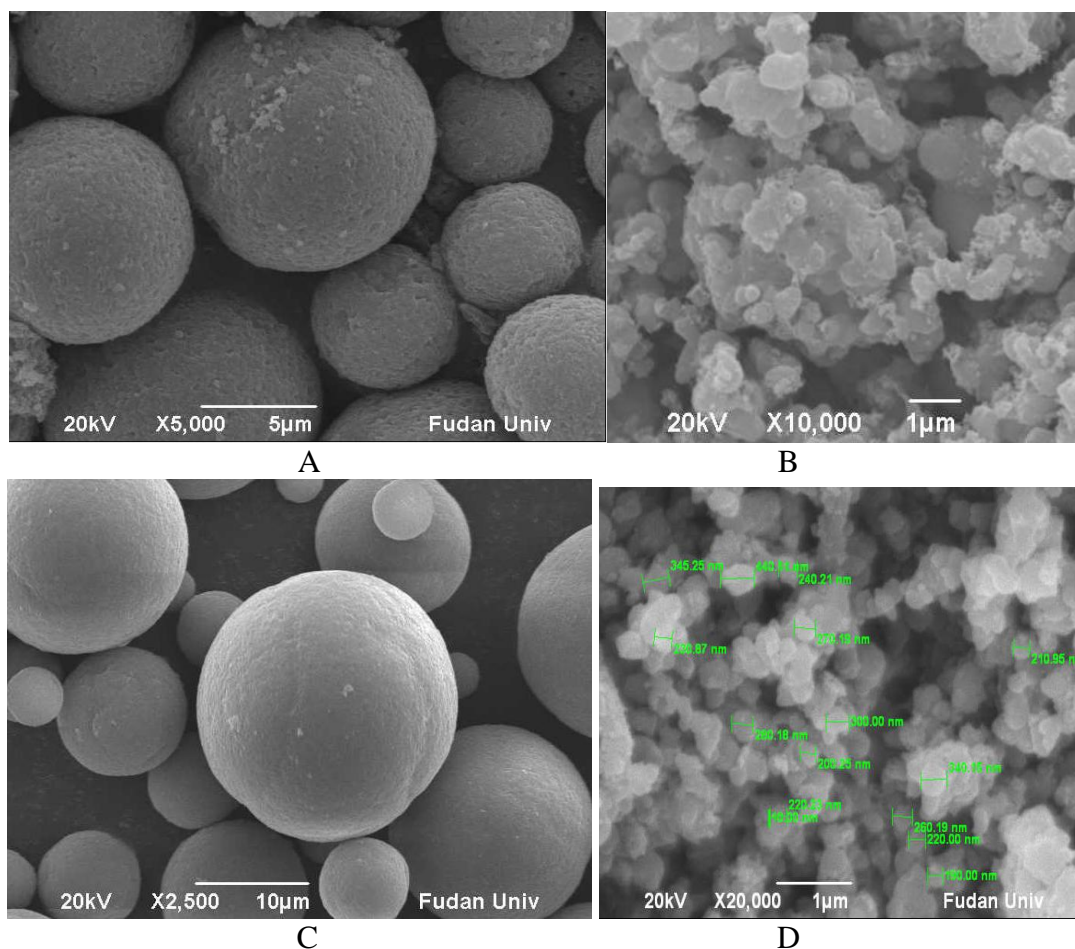

Figure 2. SEM photos for the LiFePO$_4$/C composite; a), b) LFP-400, c), d) LFP-200.

Microspheres pores were thought to form from sucrose degradation. The sucrose was well-dispersed in the precursor solution and then uniformly distributed during microsphere aggregation. Fig.

3 shows the size distribution for the powders; a) and b) as well as c) and d) depict the size distributions for the LFP-400 and LFP-200 secondary and primary particles, respectively. The singlet peaks indicate a narrow size distribution. The D50 for the LFP-400 and LFP-200 secondary and primary particles were 14.2 μm and 403 nm and 16.7 μm and 206 nm. The data are consistent with the previous SEM photos.
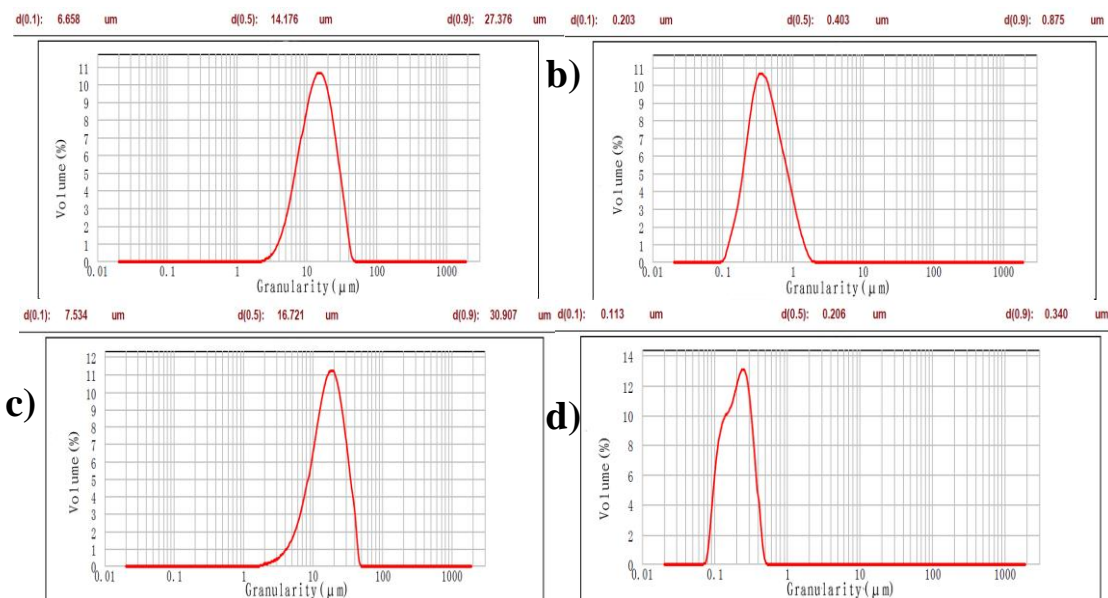

Figure 3. Size distribution for the $LiFePO_4$/C composite secondary and primary particles; a), b) LFP-400 and c), d) LFP-200.
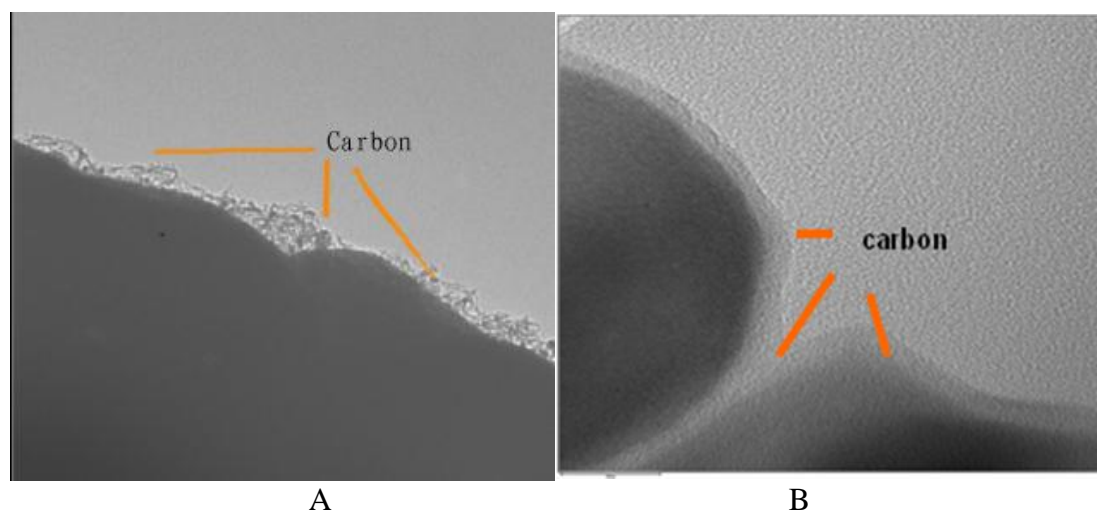

Figure 4. TEM photos for the $LiFePO_4$/C composite; a) LFP-400, b) LFP-200.

To further investigate carbon distribution in the powders, TEM characterization was performed for the samples. Fig. 4 a) and b) show TEM photos for LFP-400 and LFP-200, respectively. The

primary $LiFePO_4$ particles were wrapped in a distinct carbon layer less than 10 nm; the carbon layer was uniform and dense. To a certain extent, the carbon in the $LiFePO_4$/C composite is a key issue in determining the electrochemical performance of the battery. A thin uniform shell of carbon on the $LiFePO_4$ particles can serve as the primary pathway for electrons between interparticle contact points [21]. The carbon content in LFP-400 and LFP-200 was approximately 1.5%, which was measured using a carbon-sulfur analyzer.
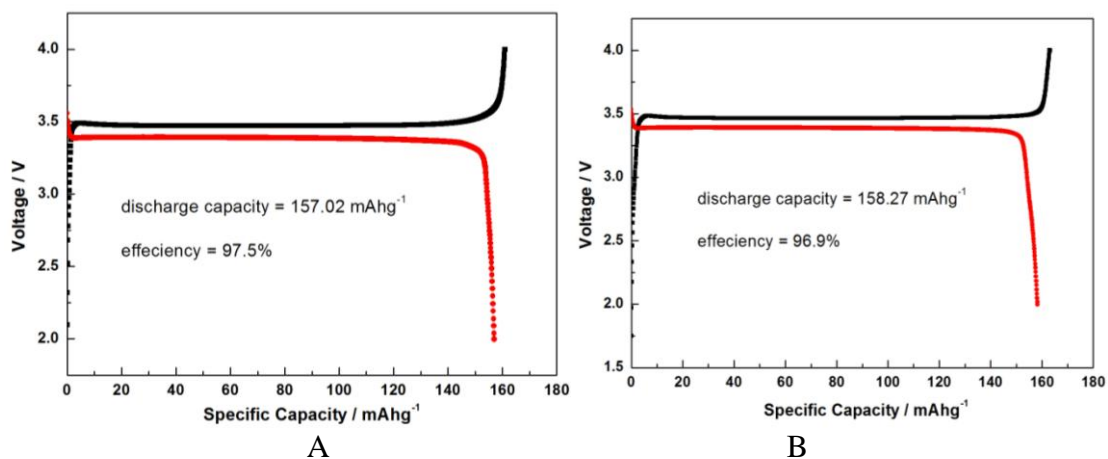
3.2 Electrochemical analysis

Figure 5. Initial discharge curves for half cells at 0.2 C with as-prepared $LiFePO_4$/C electrodes; a) LFP-400, b) LFP-200.
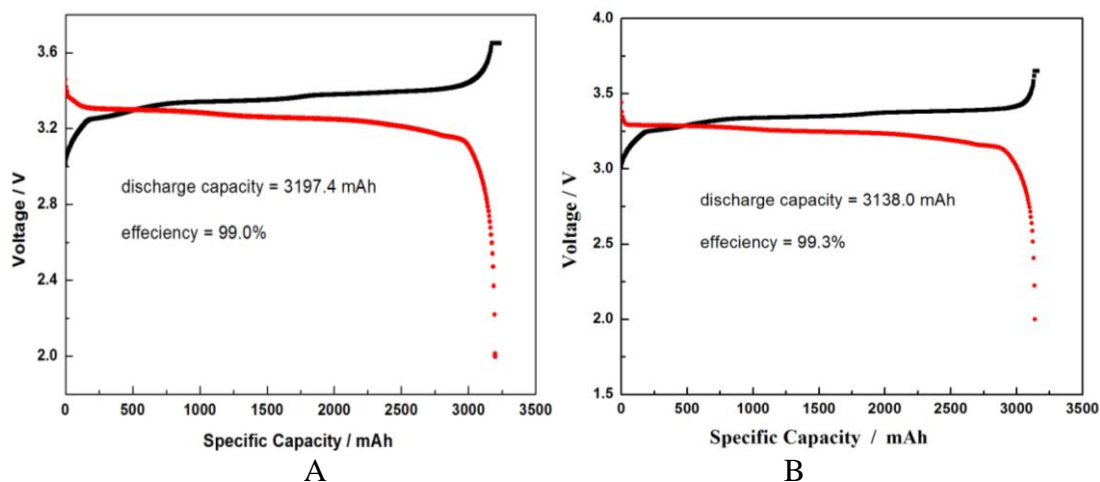

Figure 6. Initial discharge curves of full cells at 0.2 C with as-prepared $LiFePO_4$/C electrodes; a) LFP-400, b) LFP-200.

The initial charge-discharge curves for LFP-400 and LFP-200 in a coin cell are shown in Fig. 5 a) and b). Both plots show excellent plateaus at 3.5 V (vs Li) associated with the Fe^{2+}/Fe^{3+} redox

process. The voltage profiles also show a narrow gap between charge and discharge, which indicates very low electrode resistance. This could be ascribed to the uniformly distributed carbon on the particles. The discharge specific capacities for LFP-400 and LFP-200 at 0.2 C were 157.02 mAh g^{-1} and 158.27 mAh g^{-1}; the plateau time was over 95%. The initial charge-discharge efficiency was 97.5% and 96.9%. Hence, well-dispersed carbon on the LiFePO$_4$ particle surface served as a conducting 3D network, which enabled both Li$^+$ and electrons to migrate more quickly and thus fully utilized the active materials [10, 22].

The IFR26650E-3000-type full cell was employed to further investigate electrochemical performance in the LiFePO$_4$/C electrodes. The charge-discharge process was as follows: the cells were charged to 3.65 V at 0.2 C, charged at a constant 3.65 V until the current decreased to 0.05 C and then discharged to 2.0 V at 0.2 C. Fig. 6 a) and b) show the typical charge-discharge curves for LFP-400 and LFP-200, respectively. The discharge capacities were 3197.4 mAh and 3138.0 mAh at 0.2 C, and the coulomb efficiencies were both approximately 99%. The charge capacity of LFP-200 at a constant voltage charge step was smaller than that of LFP-200. This produced a shorter lithium ion moving pathway and a lower charge-discharge transfer for LFP-200 [19]. To investigate the cycling ability of these two electrodes, the full cells were both charged and discharged at 1C, and the curves are shown in Fig. 7 a) and b).
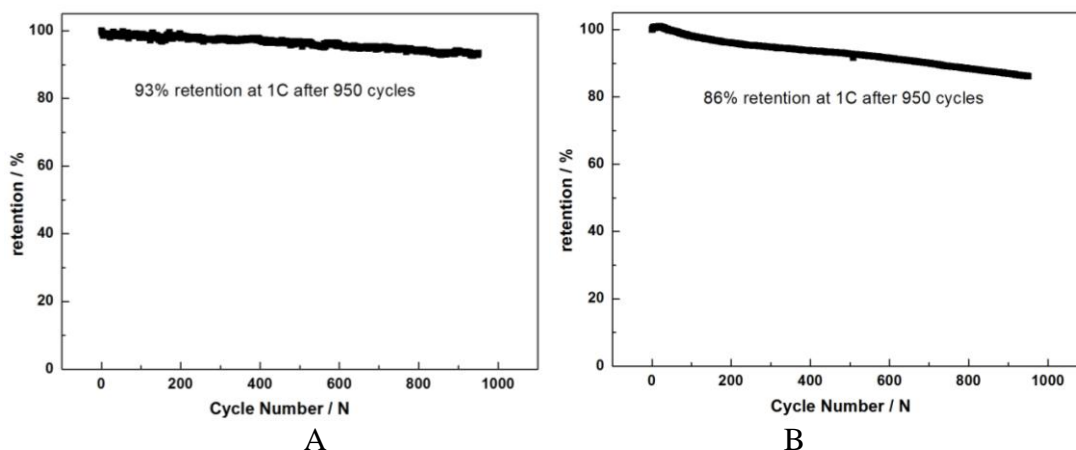

Figure 7. Cycling performance of full cells at 1 C with as-prepared LiFePO$_4$/C electrodes; a) LFP-400, b) LFP-200.

The retention capacities were 93% and 86% for LFP-400 and LFP-200 after 950 cycles, respectively. Thus, the LFP-400 electrodes had a larger discharge capacity and better cycling performance.

Fig. 8 shows retention capacity as a function of different rates for LFP-400 and LFP-200 with an IFR26650E-3000-type full cell. The cells were charged at 0.2 C to 3.65 V and then discharged to 2.0 V at a rate of n C (where n= 0.2, 0.5, 1, 2, 3). With an increase in current density, the discharge retention capacities for the two samples had different trends. The curves illustrate that the discharge capacities for LFP-400 at various rates decreased more dramatically than those for LFP-200. For

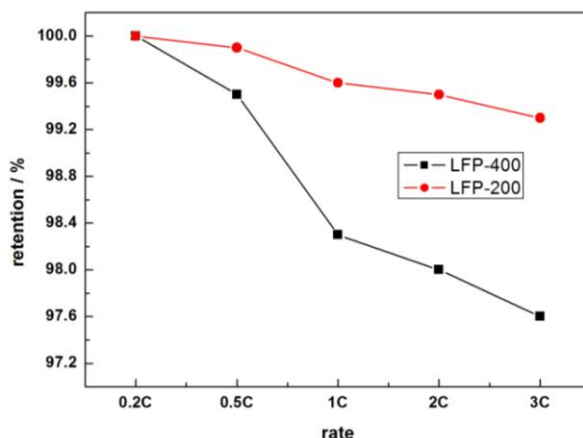example, the retention capacities at 3 C and 0.2 C for LFP-400 and LFP-200 were 97.6% and 99.3%, respectively.

Figure 8. Retention capacities for full cells at various rates with as-prepared LiFePO$_4$/C electrodes; a) LFP-400, b) LFP-200.
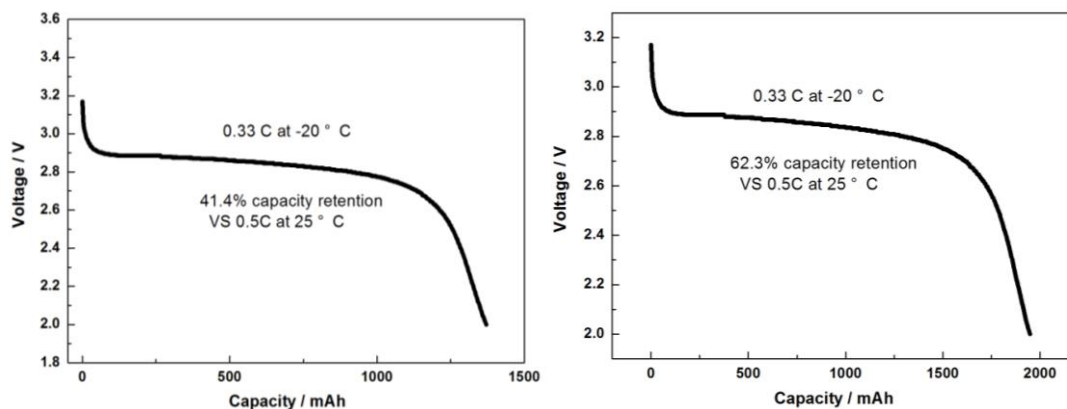

Figure 9. -20 °C discharge curves of full cells at 0.33 C with as prepared LiFePO$_4$/C electrodes; a) LFP-400, b) LFP-200.

The results show that LFP-200 had a better rate than LFP-200. It is easy to suppose that small particles could reduce the pathway for lithium ion diffusion and improve processibility in the LiFePO$_4$ cathode. Hence, the smaller particle size yielded a much better rate performance.

Low temperature performance was important in judging the electrochemical behavior of the LiFePO$_4$/C composites. Hence, the charge-discharge measurements were conducted at -20 °C for the full cells using the two electrodes. Fig. 9 a) and b) show the discharge curves for LFP-400 and LFP-200, and the plat voltage plateau is discernible. Approximately 43% and 60% capacity was maintained for LFP-400 and LFP-200 at 0.33 C compared with 0.5 C at 25 °C. The capacities were 1371.01 mAh and 1947.39 mAh. Hence, it is reasonable to conclude that LFP-400 had a higher capacity and cycling ability; however, LFP-200 had a better rate and low temperature performance.

The excellent electrochemical performance was produced through controlled LiFePO$_4$/C synthesis. The spray-drying procedure ensured a favorable nano-microstructured spherical morphology with a narrow size distribution. The spherical morphology can improve material processibility, and the surface mesopores can facilitate entrance of an electrolyte. The uniformly distributed carbon layer was developed through sucrose carbonization and featured high electronic conductivity. The SEM photos showed that the primary particle size could be successfully controlled through this procedure, which produced a particular electrochemical behavior. Generally, smaller particle sizes produced better rates and low-temperature performance.

Until now, commercial LiFePO$_4$/C composites directed to the hybrid electrical vehicle and pure electrical vehicle markets were divided into high-power and high-energy density categories. These features undoubtedly depended on the primary particle size. Hence, the realization of size-controlled LiFePO$_4$/C composite synthesis is important for commercial production.

4. CONCLUSIONS

Herein, nano-microstructured spherical LiFePO$_4$/C composites composed of nano-size primary particles were successfully synthesized through a ball-milling and spray-drying method. This unique structure could ensure a high specific surface area and improve contact between particles. We found that the size of primary particles (in diameter) could be controlled by adjusting certain parameters during production. By changing the primary particle size, the discharge capacity, cycling ability, rate capability, and low temperature performance were also different. Hence, it is reasonable to synthesize nano-microstructured spherical LiFePO$_4$/C composites with various primary particle sizes in accordance with different needs.

References

1. J.-M. Chen, C.-H. Hsu, Y.-R. Lin, M.-H. Hsiao, G.T.-K. Fey, *J. Power Sources* 184 (2008) 498-502.
2. B. Huang, P.F. Shi, Z.C. Liang, M. Chen, Y.F. Guan, *J. Alloys Compd*. 394 (2005) 303-307.
3. L. Damen, J. Hassoun, M. Mastragostino, B. Scrosati, *J. Power Sources* 195 (2010) 6902-6904.
4. Y. Wang, J. Wang, J. Yang, Y. Nuli, *Adv. Funct. Mater*. 16 (2006) 2135-2140.
5. B. Huang, X.D. Zheng, X.P. Fan, G.H. Song, M. Lu, *Electrochem. Acta* 56 (2011) 4865-4868.
6. A.K. Padhi, K.S. Nanjundaswamy, J.B. Goodenough, *J. Electrochem. Soc*. 144 (1997) 1188-1194.
7. S.Y. Chung, J.T. Bloking, Y.M. Chiang, *Nat. Mater*. 1 (2002) 123-128.
8. P.P. Prosini, M. Lisi, D. Zane, M. Pasquali, *Solid State Ionics* 148 (2002) 45-51.
9. H.C. Shin, W.I. Cho, H. Jang, *Electrochim. Acta* 52 (2006) 1472-1476.
10. D. Choi, P.N. Kumta, *J. Power Sources* 163 (2007) 1064-1069.
11. P. Subramanya Herle, B. Ellis, N. Coombs, L.F. Nazar, *Nat. Mater*. 3 (2004) 147-152.
12. M. Koltypin, D. Aurbach, L. Nazar, B. Ellis, *J. Power Sources* 174 (2007) 1241-1250.
13. A. Yamada, H. Koizumi, S.I. Nishimura, N. Sonoyama, R. Kanno, M. Yonemura, T. Nakamura, Y. Kobayashi, *Nat. Mater*. 5 (2006) 357-360.
14. M. Piana, B.L. Cushing, J.B. Goodenough, N. Penazzi, *Solid State Ionics* 175 (2004) 233-237.
15. K. Kanamur, S. Koizumi, K. Dokko, *J. Mater. Sci*. 43 (2008) 2138-2142.
16. J.G. Ren, W.H. Pu, X.M. He, C.Y. Jiang, C.R. Wan, *Ionics* 17 (2011) 581-586.

17. F. Yu, J.J. Zhang, Y.F. Yang, G.Z. Song, *J. Power Sources* 189 (2009) 794-797.
18. R. Dominko, M. Bele, M. Gaberscek, M. Remskar, D. Hanzel, J.M. Goupil, S. Pejovnik, J. Jamnik, *J. Power Sources* 153 (2006) 274-280.
19. B. Huang, X.D. Zheng, D.M. Jia, M. Lu, *Electrochim. Acta* 55 (2010) 1227-1231.
20. Q.B. Liu, S.J. Liao, H.Y. Song, Z.X. Liang, *J. Power Sources* 211 (2012) 52-58.
21. I.V. Thorat, T. Joshi, K. Zaghib, J.N. Harb, D.R. Wheeler, *J. Electrochem. Soc*. 158 (2011) A1185-A1193..
22. Y.S. Hu, Y.G. Guo, R. Dominko, M. Gaberscek, J. Jamnik, *J. Maier, Adv. Mater*. 19 (2007) 1963-1966.